A Platinum Open Access Journal for Organic Chemistry

Paper

Free to Authors and Readers

DOAJ Seal

Arkivoc **2026** (6) 202612626

Synthesis, characterization and *in-vitro* antibacterial proprieties of Mn(II) and Mg(II) complexes with azo ligand derived from *p*-acetamidophenol and benzidine

Dennue R. Kamga,[a] Joseph Tsemeugne,[b] Emmanuel F. Sopbué, [a,*] Jean-de-Dieu Tamokou,[a] André D. Siéwé,[a] Apollinaire Tsopmo,[c] Giscard Doungmo,[d] Peter F. W. Simon,[e] Bruno N. Lenta,[f] and Roger J. Kuiate[a]

[a] Univ. of Dschang, P.O. Box 67 Dschang, Republic of Cameroon; [b] Univ. of Yaounde I, P.O. Box 812 Yaounde, Republic of Cameroon; [c] Carleton Univ., 1125 Colonel By Drive K1S 5B6, Ottawa; [d] Institut für Anorganische Chemie, Christian-Albrechts-Universität zu Kiel, Max-Eyth-Str. 2, 24118 Kiel, Germany; [e] Rhine-Waal Univ. of Applied Sciences, Campus Kleve, Marie-Curie Strasse 1, D-47533 Kleve, Germany; [f] Univ. of Yaounde I; P. O. Box 47, Yaounde, Cameroon

Email: sopbue@yahoo.fr

Received 06-15-2026 **Accepted** 09-30-2026 **Published on line** 10-12-2026

Abstract

This work reports the synthesis and characterization of a novel bidentate bisazo ligand (H_2L), and its coordination compounds with Mn(II) and Mg(II) ions. Complexation in DMSO yielded compounds with the formulae $[Mn_2(L)_2(DMSO\text{-}O)_8]Cl_2{\cdot}2H_2O$ and $[Mg(H_2L)(NO_3)(DMSO\text{-}O)]NO_3$. The Mn(II) complex is a binuclear with an octahedral sphere completed by oxygen atoms from four DMSO ligands. The Mg(II) complex adopts a tetrahedral geometry, coordinated by two carbonyl oxygen atoms from the ligand, one DMSO, and one nitrate anion. The free ligand and the Mg(II) complex exhibiting potent activity (MIC of 32 µg/mL) against Escherichia coli ATCC 8739 and Staphylococcus aureus ATCC 25923, respectively.

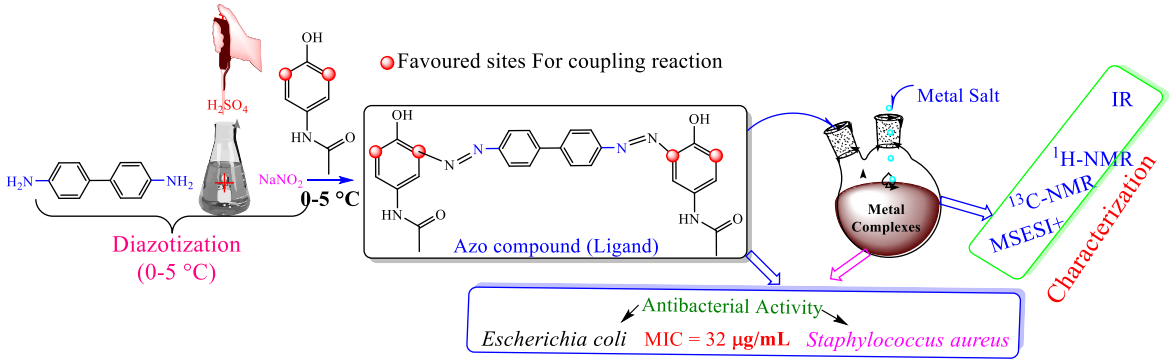

Keywords: Synthesis, azo ligands, *p*-acetamidophenol, metal complexes, antibacterial activity

Cite as *Arkivoc* **2026** (6) 202612626

DOI: https://doi.org/10.24820/ark.5550190.p012.626

©AUTHOR(S)

Introduction

Coordination chemistry, especially of transition metals, offers a powerful platform for developing compounds with tailored physical, chemical, and biological properties.[1-4] The ability to synthesize complexes with organic azo ligands is particularly fascinating, as their structures can be precisely modulated for specific applications in catalysis, optics, and medicine.[2,5] Arylazophenol ligands exemplify this versatility; their inherent N- and O-donor atoms enable them to chelate various metal ions, forming highly stable complexes.[6-9] Moreover, the biological activity of these ligands can be enhanced upon coordination with metals, further expanding their potential applications.[1-7,9] This study focuses on a novel bisazo ligand synthesized from *p*-acetamidophenol and benzidine. *p*-Acetamidophenol is a widely used analgesic and antipyretic,[10] while benzidine derivatives are common building blocks for biologically active compounds.[4-5] We think that merging these two pharmacophores will result in a ligand that combines their intrinsic biological characteristics.[4-5,11-12] Moreover, coordinating this hybrid ligand to a metal center is expected to further enhance its activity, a well-established phenomenon in medicinal inorganic chemistry where drug repurposing is a promising strategy.[13]

We selected Manganese (II) and Magnesium (II) for complexation. Mn(II), a first-row transition metal, typically forms stable, six-coordinate complexes with N,O-donor sets.[2,14] Magnesium, an s-block element, also forms stable four- or six-membered chelates.[11] While both free metal ions play roles in biological catalysis, their chelation often significantly boosts bioactivity. This is evident in nature, where many essential enzymes are metalloproteins.[11-12] Importantly, metal complexes are frequently more potent against microorganisms than the free ligands alone,[1,3-4,11] a trend observed with previous *p*-acetamidophenol-derived azo complexes.[1,8]

Driven by these considerations, we report the synthesis and characterization of new Mn(II) and Mg(II) complexes with a bisazo ligand derived from *p*-acetamidophenol and benzidine. This research aims to evaluate the antimicrobial potential of these complexes, advancing the development of new metal-based agents to combat infectious diseases. All the above prompted us to synthesize new Mn(II) and Mg(II) complexes using a bisazo ligand derived from *p*-acetamidophenol, in order to evaluate their antimicrobial activity. Given the proven biological applications of complexes derived from *p*-acetamidophenol and benzidine with other metals, this research aims at pursuing our investigations on the development of new antimicrobial agents based on new coordination complexes from organic ligands which could effective against infectious diseases.

Results and Discussion

Chemistry

The synthesis of ligand (H_2L) (**4**) and its metal complexes followed the pathways detailed in Schemes 1 and 2. Complexation of H_2L with $MnCl_2$ and $Mg(NO_3)_2$ in DMSO, using 2:2 and 1:1 metal:ligand ratios, afforded the complexes $[Mn_2(L)_2(O\text{-}DMSO)_8]Cl_2\cdot 2H_2O$ and $[Mg(H_2L)(NO_3)(O\text{-}DMSO)]NO_3$**,** respectively. The resulting complexes were obtained as air-stable solids, soluble in various organic solvents including DMSO, ethanol, and acetone. The molecular structure of the ligand and the proposed coordination geometries for both complexes (binuclear octahedral Mn(II) center and mononuclear Mg(II) center) were unequivocally confirmed by elemental analysis (Table 1), FT-IR spectroscopy (Table 2), and $^1H/^{13}C$-NMR spectroscopy (Tables 3 and 4).

 ©AUTHOR(S)

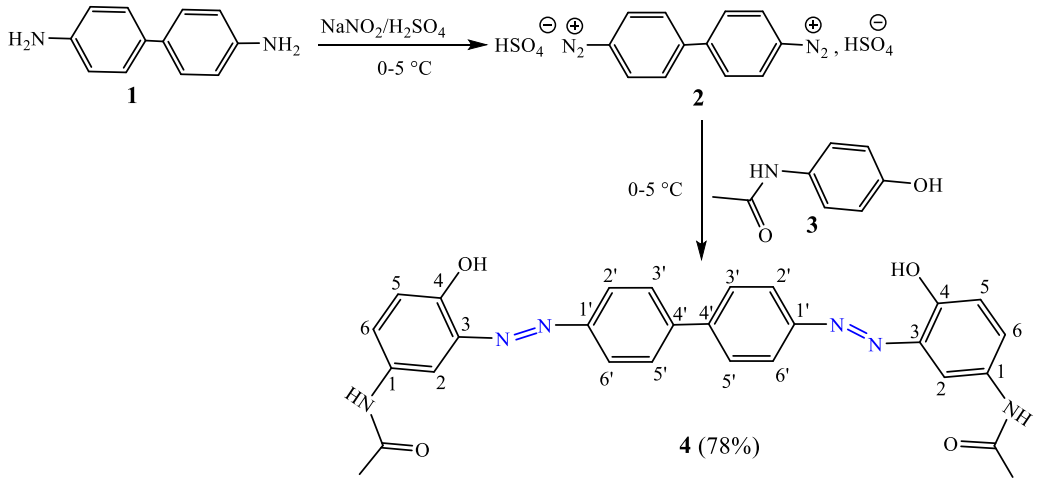

Scheme 1. Reaction pathway to ligand **4.**

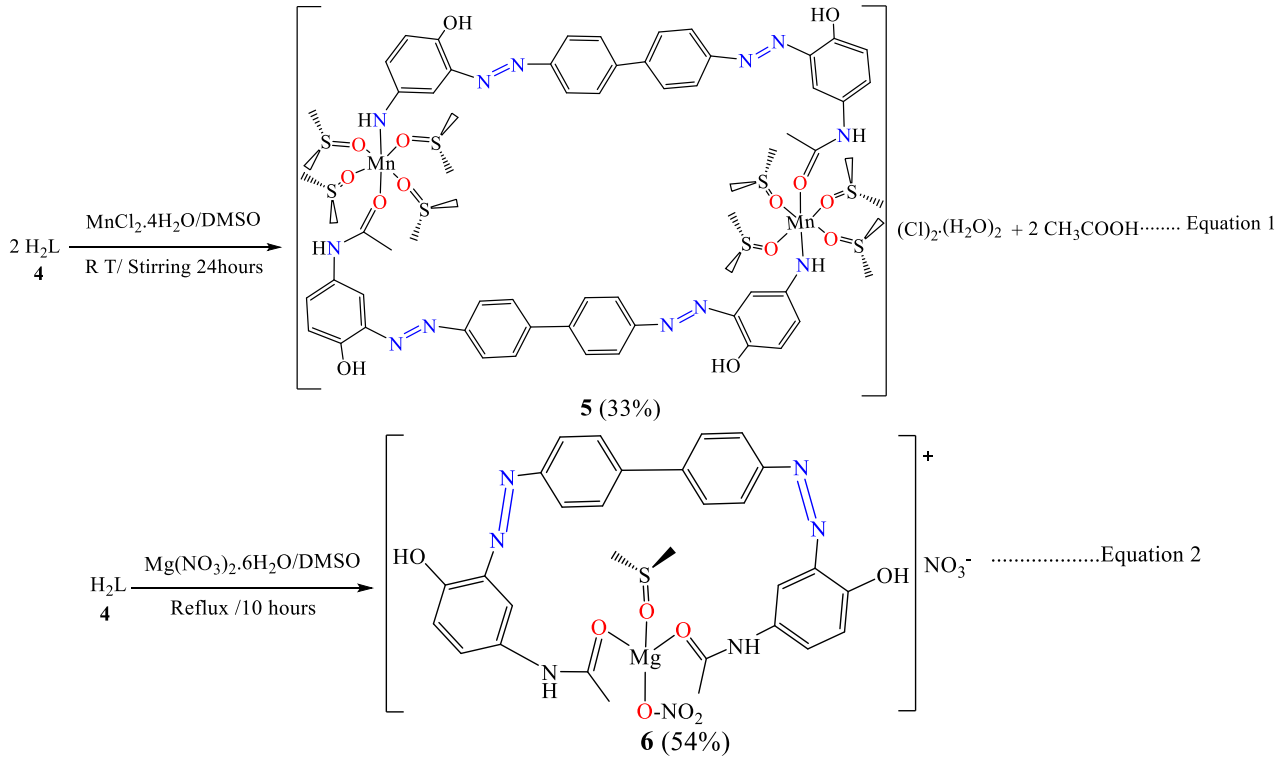

Scheme 2. Reactions' sequences for the preparation of complexes **5** and **6.**

 ©AUTHOR(S)

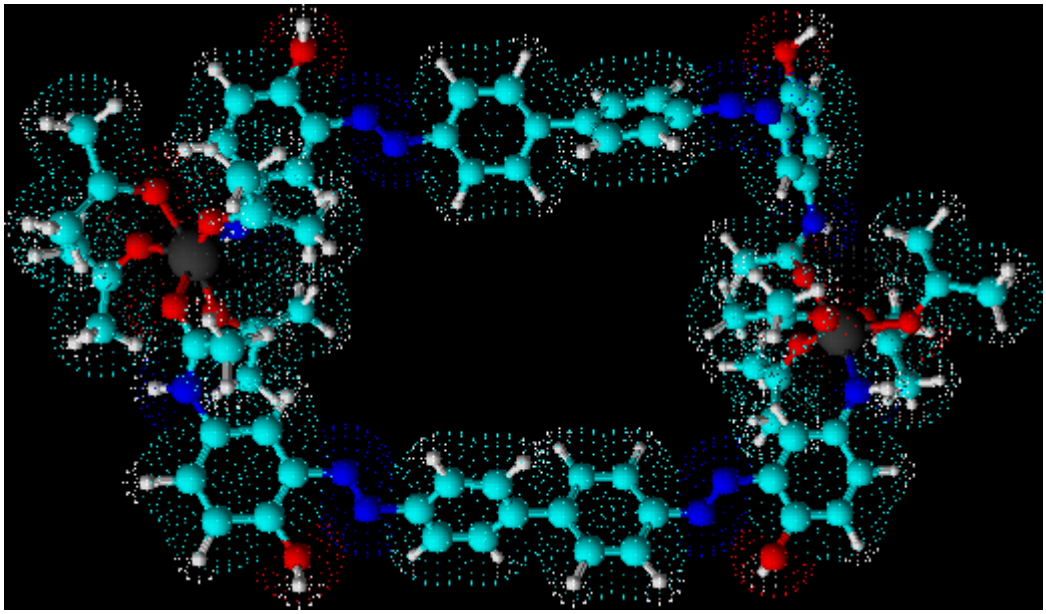

Figure 1. Optimized 3D view of the coordination spheres of **5** drawn with ACD/Labs 3D viewer (freeware).

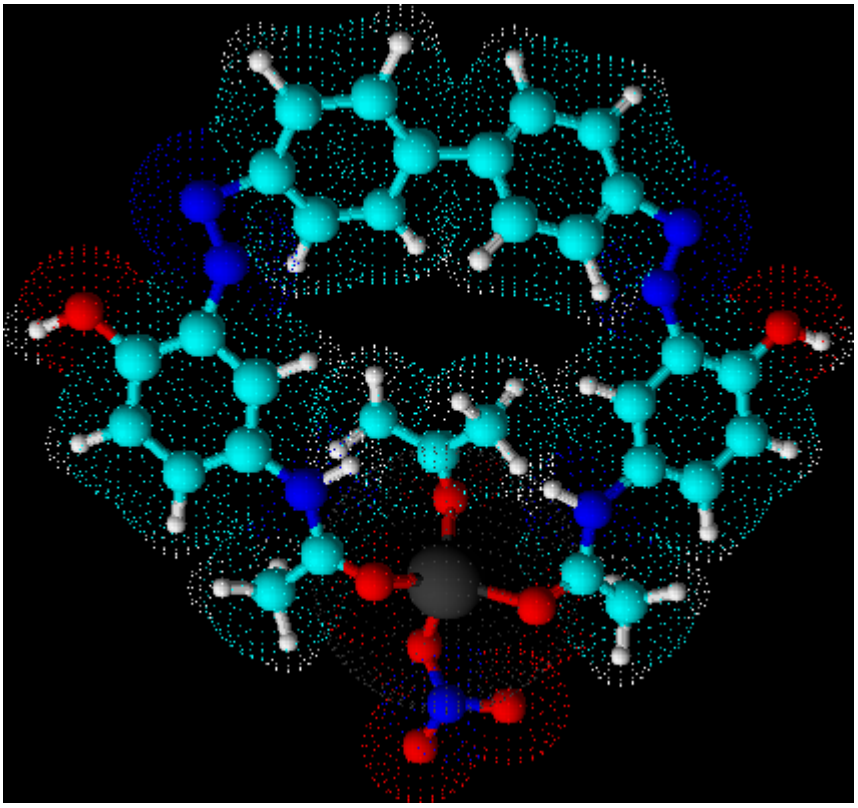

Figure 2. Optimized 3D view of the coordination spheres of **6** drawn with ACD/Labs 3D viewer (freeware).

 ©AUTHOR(S)

Table 1. Physical and analytical data of the ligand (**4**) and its new metal complexes (**5** and **6**)

Compounds (Formula)	Colour	%Yield	Calculated (Found), %			
			C	H	N	S
Ligand (H_2L) **4** $C_{28}H_{24}N_6O_4$	Dark red powder	78	66.13 (66.12)	4.76 (4.71)	16.53 (16.57)	-
Complex **5** $[Mn_2(L)_2(O\text{-}DMSO)_8])(Cl)_2.2H_2O$	Red powder	33	46.07 (46.17)	5.34 (5. 39)	9.48 (9.33)	14.47 (14.58)
Complex **6** $[Mg(H_2L)(O\text{-}NO_2)(O\text{-}DMSO)](NO_3)$	reddish powder	54	49.03 (49.18)	4.11 (4.17)	15.25 (15.37)	4.36 (4.47)

IR Spectra of Ligand 4 and Metal Complexes 5 and 6: The infrared spectra of the metal complexes were compared with that of the free ligand **(H_2L, 4)** to identify coordination sites (Figures 1 and 2, Table 2). The ligand IR spectrum exhibits characteristic bands at 3266 cm^{-1} (intramolecular phenolic OH---N), 1652 cm^{-1} (C=O), and 1490 cm^{-1} (symmetric N=N).[14-15] In the complexes, key shifts and new bands reveal the coordination mode. The O-H (broad band at ~3270-3288 cm^{-1}) vibration indicate the phenolic oxygen does not coordinate.[7,14,16-17] These is confirmed by C-O (1270 cm^{-1}) that remains unchanged.[7] In addition, the unchanged azo N=N band (1490 cm^{-1}) also rules out its involvement.[5,14,16,18] Furthermore, a shift in the C=O stretch from 1652 cm^{-1} to 1660 cm^{-1} confirms coordination through the carbonyl oxygen atom, establishing the ligand's bidentate nature.[14,19-20] New bands at 949 and 952 cm^{-1} for complexes **5** and **6**, respectively, are assigned to the S=O stretch of O-bonded DMSO, ruling out S-coordination, that should be displayed at higher wave number (≈1000 cm^{-1}) than the first one.[21-23] Based on previous findings[21] on the prevalence of O-bonding and S-bonding in metal sulfoxide complexes, all the factors governing the coordination bonding mechanism are favorable for the DMSO O-bonding in compounds **5** and **6**. The appearance of new bands in the 600-400 cm^{-1} region confirms metal-heteroatom bonding. For the Mn(II) complex (**5**), bands at 572 and 437 cm^{-1} are assigned to Mn-O and Mn-N bonds, respectively. For the Mg(II) complex (**6**), the Mg-O bond is observed at 572 cm^{-1}.[6,17] Finally, nitrate coordination in Mg(II) complex (**6**) are justified by three additional novel bands at 1547, 1430, and 1249 cm^{-1} attributed to nitrate υ_a(N=O) and υ_s(N-O) vibrations. The separation (Δν) of 117 cm^{-1} between the asymmetric and symmetric stretches (υ_a and υ_s) is consistent with a monodentate coordination mode.[19,20] Collectively, the IR data confirm the ligand acts as a bidentate donor via the carbonyl oxygen, with additional coordination from DMSO and, in the case of complex **6**, a monodentate nitrate ion.

 ©AUTHOR(S)

Table 2. Selected IR bands (cm^{-1}) of the ligand and their metal complexes

Compounds	O-H	C=O	N=N	υ_a (N=O)	υ_s (N-O)	S=O	M-O	M-N
Ligand **4**	3266	1652	1490	-	-	-	-	-
Complex **5**	3278	1660	1490	-	-	949	572	437
Complex **6**	3288		1490	1547, 1430	1246	952	572	-

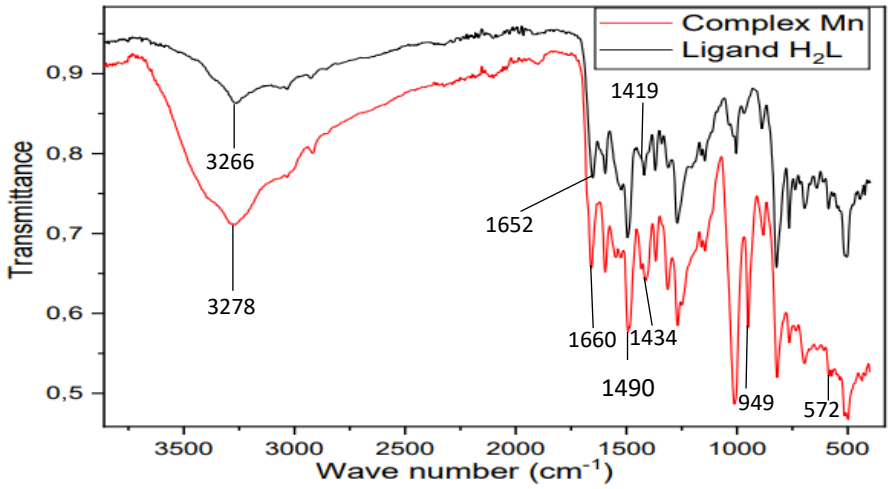

Figure 3. Comparative IR spectrum of complex **5** (red) with that of ligand **4** (black).

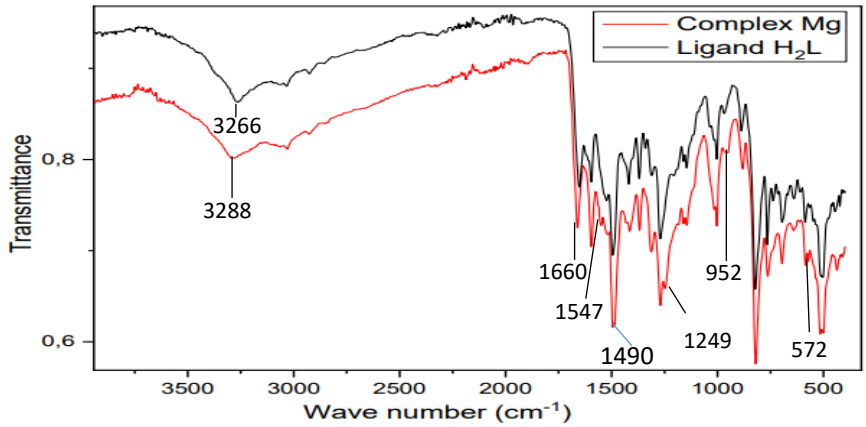

Figure 4. Comparative IR spectrum of complex **6** (red) with that of ligand **4** (black).

NMR assignments of ligand 4 and metals complexes 5 and 6: NMR spectroscopy confirmed the symmetric structure of ligand **4** and provided key insights into the coordination geometry of its metal complexes. The ^{1}H-NMR spectrum (Figure 3) of the ligand (H_2L, **4**) is consistent with a symmetric structure. Key signals include aromatic multiplets (δ_H 8.09-7.00), including a signal at δ_H 7.00 (*d*, 2H, J_o = 8.8 Hz, H-5), 7.55 (*dd*, 2H, J_o = 8.8 Hz, J_m = 2.4 Hz, H-6), 8.03 (*d*, 2H, J_m = 2.4 Hz, H-2). two singlets for exchangeable protons at δ_H 10.72 (*s*, 2H, OH) and 9.93 (*s*, 2H, NH), and a singlet at δ_H 2.01 (6H, $NHCOCH_3$) confirming the *p*-acetamidophenol moiety.[7] The symmetry is evidenced by the equivalent integrals and the doublet signals at δ_H 8.09 (*d*, 4H, J_o= 8.4 Hz, H-3'/H-5') and 7.99 (*d*, 4H, J_o = 8.4 Hz, H-2'/H-6') for the *p*-substituted benzidine rings.[4,7] The ^{13}C-NMR spectrum (figure 4) further confirms this symmetry, displaying only 12 distinct signals for the 24 carbon atoms. The

 ©AUTHOR(S)

signals were fully assigned, with the carbonyl of the acetamido group at δ_C 168.6 and the methyl carbon at δ_C 24.4. The COSY spectrum confirmed the substitution pattern on the trisubstituted ring. So, the correlation square between H-5 (δ_H 7.00), H-6 (δ_H 7.55) and H-2 (δ_H 8.03) confirmed that copulation took place in the ortho position of the phenolic OH group.

Comparison of the complexes' ^{1}H-NMR spectra (Figures 3 and 4) with the free ligand revealed critical changes indicative of coordination. The shift of the acetamide methyl signal from δ_H 2.01 to 2.12/2.13 ppm in complexes **5** and **6**, respectively, confirms the involvement of the carbonyl in metal binding. Intense singlets at δ_H 2.64 (48H, complex **5**) and 2.62 (6H, complex **6**) are assigned to the methyl groups of O-bonded DMSO.[21] The downfield shift from free DMSO (δ_H ~2.50) and the absence of a larger shift rule out S-coordination.[22] The integrals confirm eight and one DMSO molecules per complex formula unit, respectively. Overall, the molecule remains symmetrical, as the presence of the singlet proves that all the methyl groups in DMSO are chemically equivalent. In addition, For the Mn(II) complex (**5**), the integration ratio of aromatic to methyl protons (6H/28H), indicates the loss of one acetamide group. This hydrolysis is attributed to the Lewis acidity of DMSO under the reaction conditions, as illustrated in Scheme 3.[24]

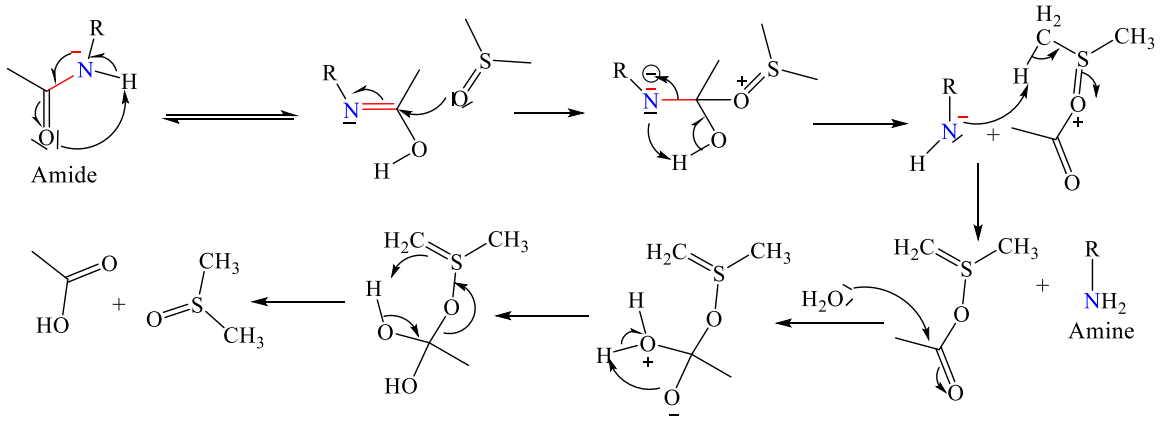

Scheme 3. Mechanism of the Lewis acid hydrolysis of the amid group of ligands **4** by DMSO.

^{13}C-NMR (figure 5b&5c) analysis of the complexes confirmed coordination via the ligand's carbonyl group and the DMSO solvent. While the aromatic carbon signals remained largely unchanged from the free ligand, the carbonyl (C=O) signal experienced a characteristic downfield shift to δ_C 170.1 and 170.3 ppm in complexes **5** and **6**, respectively.[25-26] The appearance of new signals in the complexes at 38.7 and 39.5 ppm is attributed to the methyl carbons of O-coordinated DMSO.[21-22] This assignment was supported by HMBC correlations, and the complete carbon assignment for the ligand was achieved using HSQC and HMBC spectra (Figure 6).

Table 3. ^{1}H-NMR Spectral Data of Ligand **4** and its metal complexes (**5** and **6**)

Compounds	OH	NH	Aromatics protons	Aliphatic CH_3	
				$NHCOC\underline{H}_3$	$(CH_3)_2S{=}O$
Ligand **4**	10.72	9.93	8.09-7.00	2.01 (*s*)	-
Complex **5**	-	-	8.16-6.95	2.13 (*s*)	2.64 (*s*)
Complex **6**	-	-	8.16-6.92	2.12 (*s*)	2.62 (*s*)

 ©AUTHOR(S)

Table 4. ^{13}C-NMR Spectral Data of ligand **4** and its metal complexes **(5** and **6)**

Ligand/complex	C=O	Aromatic Carbons	$\underline{C}H_3CO$-	$(\underline{C}H_3)_2S=O$
Ligand **4**	168.6	112.6-151.7	24.4	-
Complex **5**	170.1	107.7-149.4	22.3	38.7
Complex **6**	170.3	107.7-149.4	22.8	39.5

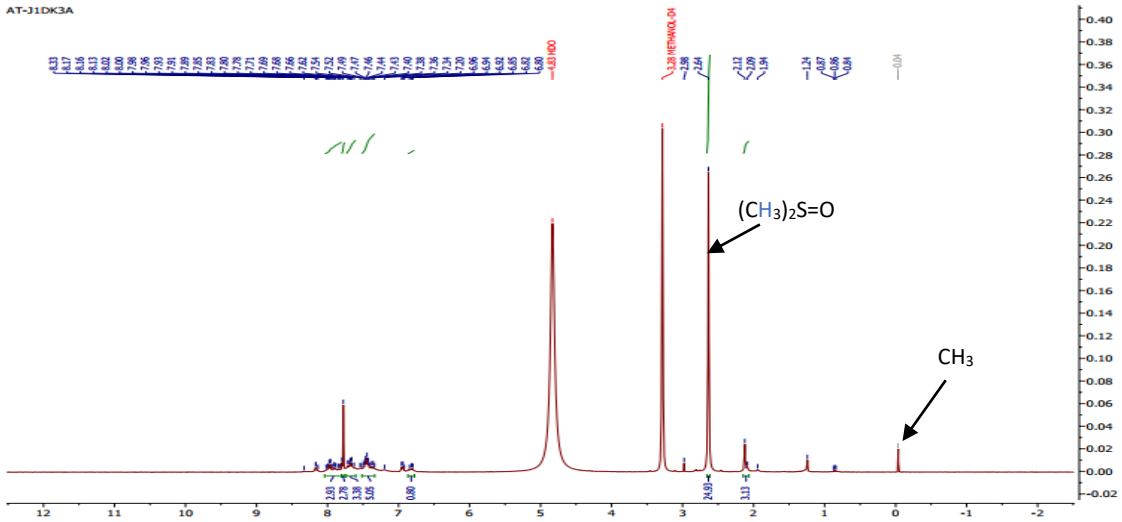

Figure 5. ^{1}H-NMR spectrum of metal complex **5.**

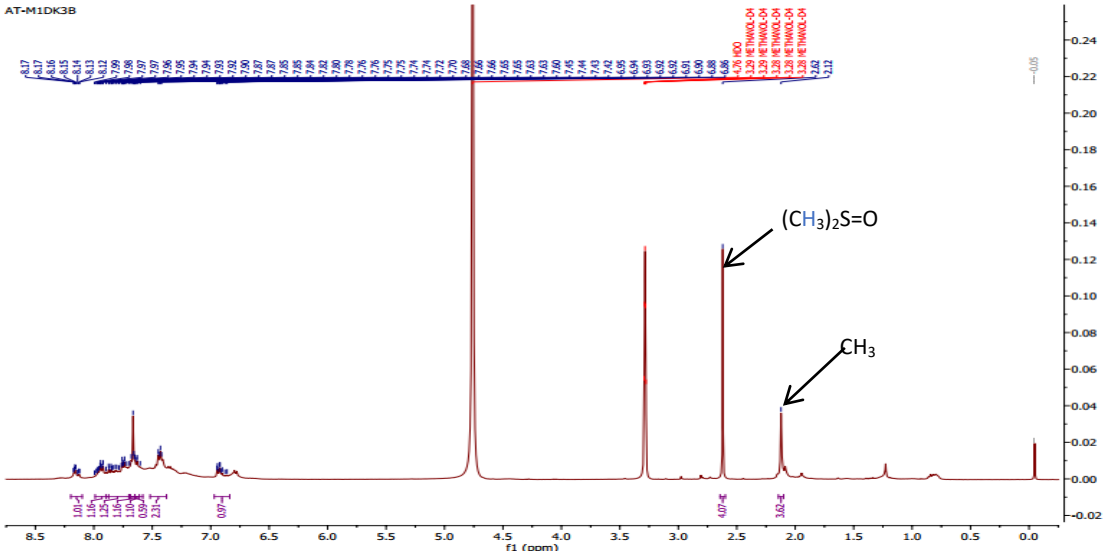

Figure 6. ^{1}H-NMR spectrum of metal complex **6.**

 ©AUTHOR(S)

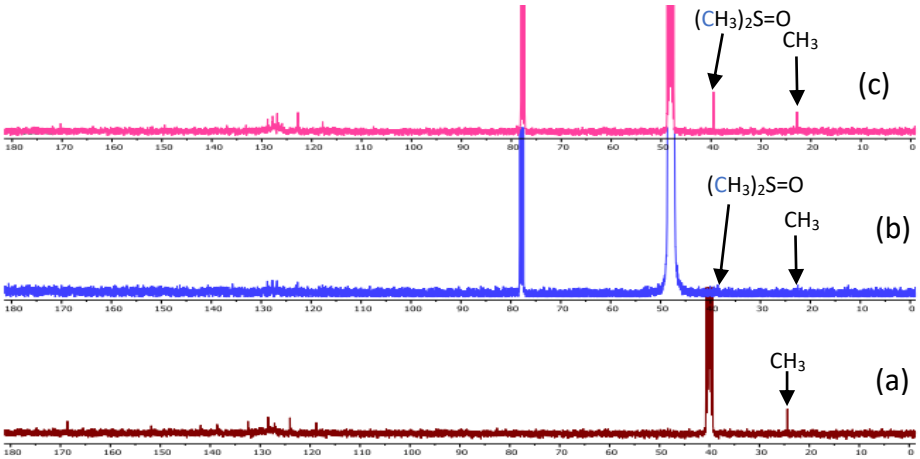

Figure 7. ^{13}C-NMR spectra of ligand **4** (red) compared with those of metal complexes **5** (blue) and **6** (pink color).

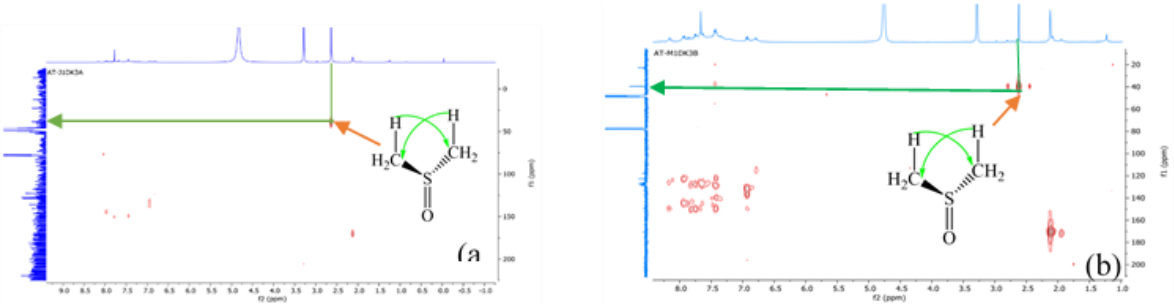

Figure 8. HMBC spectra of metal complexes **5** (a) and **6** (b).

Mass spectrometry and Fragmentation patterns: High-resolution ESI+ mass spectrometry confirmed the molecular structures of the ligand and its complexes. The spectrum of ligand **4** showed a peak ion **[M + Li]$^+$** at *m/z* 515.2048. The proposed formula for the Mn(II) complex **5** was verified by multiple ions in its mass spectrum (Figure 7a), including [M – $C_{24}H_{16}N_4O_2$ + 2H]$^{\bullet+}$ at *m/z* 1380.6169 and [$C_{17}H_{37}MnN_4O_6S_4$]$^{3\bullet+}$ at *m/z* 567, supporting the fragmentation pathway in Scheme 5. For the Mg(II) complex **6** (Figure 7b), we observed a prominent peak such as the doubly charged ion **[M + 2H]$^{2\bullet+}$** at *m/z* 736.1742 and other characteristic fragments were consistent with the structure and its proposed fragmentation (Scheme 4).

 ©AUTHOR(S)

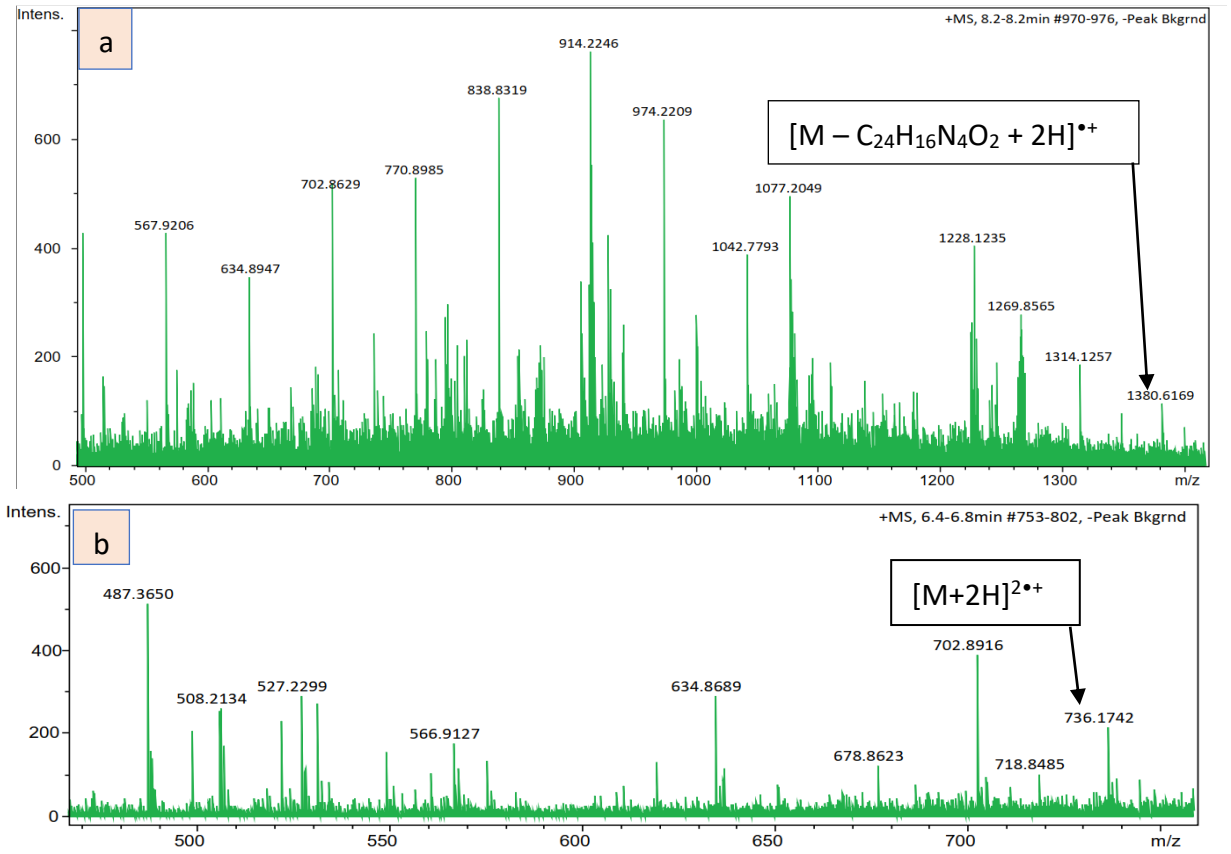

Figure 9. (ESI+) mass spectra of the metal complexes **5** (a) and **6** (b).

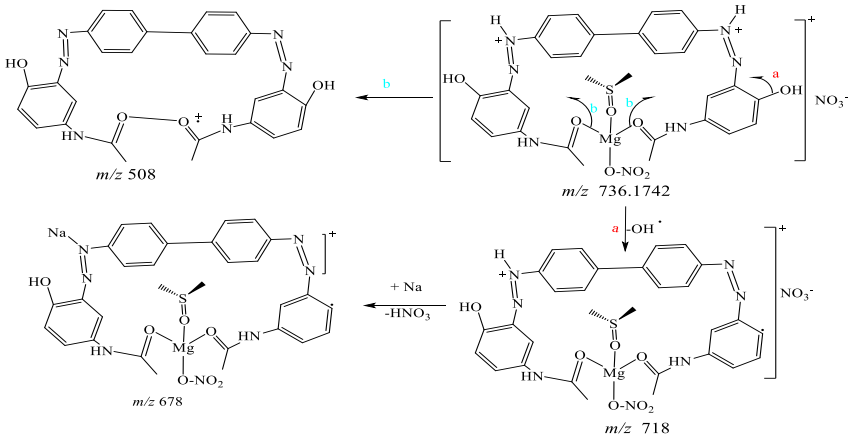

Scheme 4. Fragmentation pattern of the metal complex **6.**

 ©AUTHOR(S)

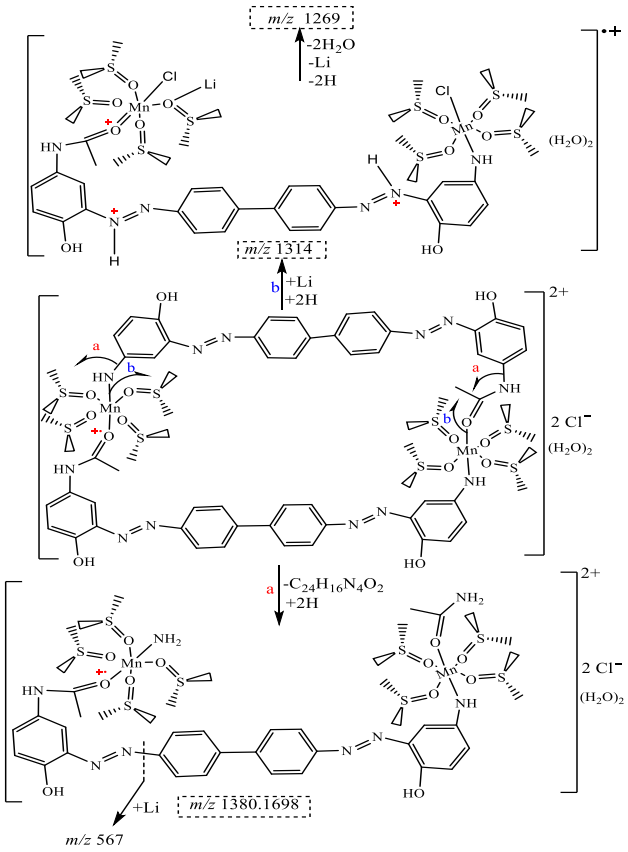

Scheme 5. Fragmentation pattern of metal complex **5.**

Computational Studies: The stability, chemical reactivity, and potential biological activity of a molecule can be predicted computationally prior to synthesis using parameters such as Frontier Molecular Orbital (FMO) energies. These were calculated for ligand 4 using DFT at the B3LYP/6-311++G(d,p) level of theory.[27] The chemical reactivity is inversely related to the HOMO-LUMO energy gap. A small gap facilitates charge transfer and indicates higher chemical reactivity and lower kinetic stability.[27,28] For ligand **4**, the calculated HOMO and LUMO energies are -5.692 eV and -2.625 eV, respectively, resulting in a narrow energy gap of 3.067 eV (Figure 8a). This low value confirms a high degree of polarization and suggests significant chemical reactivity, which is favorable for charge transfer interactions.[27, 28]

To identify specific reactive sites, the Molecular Electrostatic Potential (MEP) was mapped (Figure 8b). The MEP surface reveals regions of high electron density (red), such as the carbonyl oxygen, phenolic oxygen, and the azo nitrogen near the phenolic group, which are susceptible to electrophilic attack. Conversely, regions of low electron density (blue) are targets for nucleophiles. Furthermore, a decreased HOMO-LUMO gap in metal complexes compared to their free ligand is often associated with enhanced biological activity,[28] suggesting that coordination could potentially amplify this property in complexes derived from ligand **4**.

 ©AUTHOR(S)

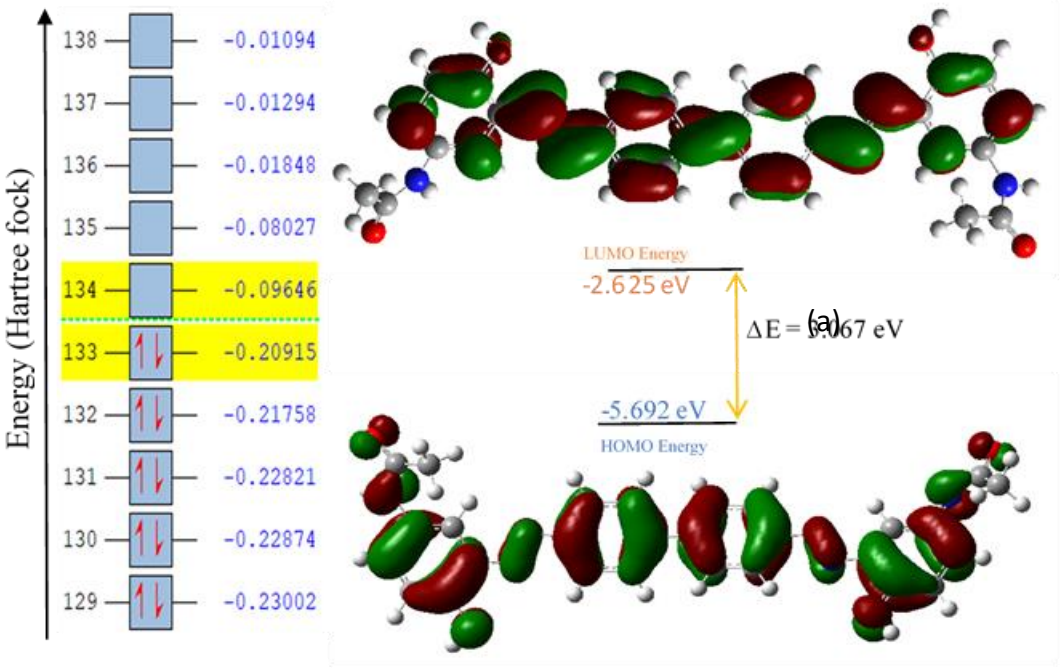

(a)

MEP

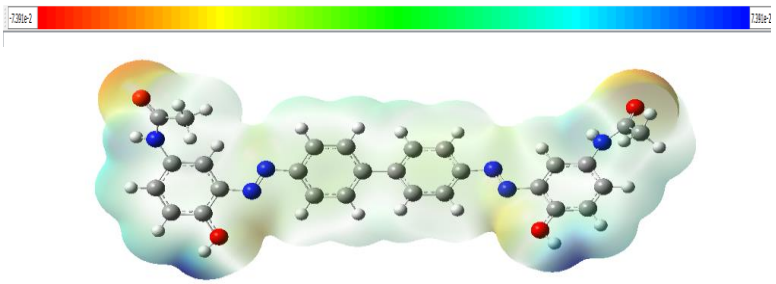

(b)

Figure 10. Energies gap of the HOMO-LUMO (a) and MEP diagram (b) of ligand **4.**

Biological

The antibacterial activities of ligand **4** and its metal complexes **5** and **6** were evaluated against Gram-positive and Gram-negative bacterial strains (Table 5). All compounds exhibited antibacterial effects, with minimum inhibitory concentrations (MICs) ranging from 32 to 128 µg/mL. Ligand **4** demonstrated moderate activity (MIC = 32-64 µg/mL) against *E. coli*, *K. pneumoniae*, and *S. aureus*, but lower activity (MIC = 128 µg/mL) against *S. Typhi* ATCC 6539.[29-31] Upon complexation, the activity profile changed significantly. The metal complexes showed enhanced potency against certain strains; for instance, both complexes were more effective against *S. aureus* (MIC = 32 µg/mL) and *S. Typhi* (MIC = 64 µg/mL) than the free ligand. Conversely, their activity was reduced against other microorganisms. Based on the MBC/MIC ratios (Table 5), ligand **4** and complex **5** exhibited a bactericidal effect (MBC/MIC ≤ 4) against all tested strains. Complex **6** was also bactericidal against most strains but showed a bacteriostatic effect (MBC/MIC = 8) against *S. aureus*.[29-32] The variation in antibacterial efficacy can be explained by the enhanced lipophilicity imparted by chelation.

 ©AUTHOR(S)

According to the Overtone's Concept of cell permeability, coordination of the metal ion to the N,O-donor ligand reduces the metal's polarity through charge delocalization. This increases the complex's lipophilicity, facilitating its passage through the bacterial lipid membrane.[8,11,19,33,34] Once inside, the complex can disrupt essential cellular processes, such as enzyme function or respiration, ultimately inhibiting growth.[35] The distinct activities of complexes **5** and **6**, despite sharing the same ligand, are attributed to the specific nature of the central metal ion and its associated counterions, which further modulate the compound's overall physicochemical properties and interaction with microbial cells.[33]

Table 5. Antibacterial activities of ligand **4** and metals complexes **5** and **6**

Microorganisms	Inhibition	Parameters			Reference drug
		Ligand **4**	Complex **5**	Complex **6**	Ciprofloxacin
E. coli ATCC 8739	MIC	32	64	128	4
	MBC	128	128	>256	4
	MBC/MIC	4	2	-	1
S. aureus ATCC 25923	MIC	64	128	32	2
	MBC	128	256	256	4
	MBC/MIC	2	2	8	2
*S.*Typhi ATCC 6539	MIC	128	64	128	2
	MBC	128	128	>256	4
	MBC/MIC	1	2	-	2
K. pneumoniae 22	MIC	64	128	128	2
	MBC	128	256	>256	4
	MBC/MIC	2	2	-	2

Ligand and complexes were not active at concentrations up to 256 µg/mL; ciprofloxacin is used as standard drug for bacteria; MIC: Minimum Inhibitory Concentration; MBC: Minimum Bactericidal Concentration

Conclusions

This work successfully demonstrates the synthesis and characterization of a new azo ligand and its corresponding Mn(II) and Mg(II) complexes, with geometries assigned as octahedral and tetrahedral, respectively. The antibacterial assessment revealed that metal coordination does not uniformly enhance activity but rather selectively modulates it based on the metal ion and the bacterial target. The observed trends including the bactericidal action of most compounds and the bacteriostatic behavior of the Mg(II) complex against *S. aureus* are attributed to the distinct physicochemical properties imparted by each metal center and the differing permeability of microbial cell walls. Ultimately, these findings confirm that coordination chemistry is a powerful tool for tuning bioactivity, capable of both augmenting and suppressing the properties of a parent ligand.

 ©AUTHOR(S)

Experimental Section

General. Commercial reagents and solvents (Sigma-Aldrich, Fluka) were employed as received. Analytical TLC was performed on silica gel 60 F254 plates with an ethyl acetate/hexane (4:6) eluent system, with visualization under UV light and iodine vapor. Characterization of the synthesized compounds included: melting point (Stuart Scientific SMP20); UV-Vis spectroscopy (UNICAM UV 300, 200-1000 nm); FT-IR spectroscopy (Bruker Alpha, ATR mode); and NMR spectroscopy (Bruker 400 MHz, with chemical shifts reported in ppm relative to TMS). The chemical shifts (δ) and coupling constants (J) are expressed in ppm and hertz respectively. High-resolution mass spectrometry (HRMS-ESI) was conducted on a BRUKER Compact instrument, and elemental analysis (CHNS-O) was performed on a Euro Vector EA 3000 or vario Micro Cube analyzer. The antibacterial activity was assessed against a panel of reference bacterial strains: *Escherichia coli* ATCC 8739, *Salmonella Typhi* ATCC 6539, *Klebsiella pneumoniae* 22 (Gram-negative), and *Staphylococcus aureus* ATCC 25923 (Gram-positive). The minimum inhibitory concentration (MIC) and minimum bactericidal concentration (MBC) were determined according to established microdilution protocols.[8,28-34] Briefly, bacterial strains were cultured in Mueller Hinton Broth (MHB). Test compounds were prepared in 5% (v/v) aqueous DMSO. In a 96-well plate, serial dilutions of the compounds were inoculated with a standardized bacterial suspension and incubated at 37 °C for 24 h. Following incubation, bacterial growth was detected by the addition of *para*-iodonitrotetrazolium violet; a change from yellow to purple indicated viable bacteria. The MIC was recorded as the lowest compound concentration that inhibited this color change. To determine the MBC, aliquots from wells showing no visible growth were subculture on Mueller Hinton Agar. The MBC was defined as the lowest concentration resulting in no bacterial growth or the growth of a single colony upon subculture. Ciprofloxacin served as the positive control, and all experiments were conducted in triplicate to ensure reproducibility.

***N,N'*-(((1*E*,1'E)-[1,1'-biphenyl]-4,4'-diylbis(diazene-2,1-diyl))bis(4-hydroxy-3,1-phenyl)) diacetamide (4) H_2L.** The targeted azo ligand, was synthesized as a dark red powder with a yield of 78% via a diazotization coupling reaction, as illustrated in the literature (Scheme 1).[4-6,26,35] Benzidine (1.84 g, 10 mmol) and sodium nitrite (1.38 g, 20 mmol) were dissolved in dimethyl sulfoxide (DMSO, 12 mL) and cooled to 0–5 °C in an ice-salt bath. Concentrated sulfuric acid (2.0 mL) was added dropwise with vigorous stirring. The resulting mixture was stirred for an additional hour at 0–5 °C to ensure complete diazotization. In a separate vessel, *p*-acetamidophenol (3.20 g, 20 mmol) was dissolved in DMSO (15 mL) and cooled to below 5 °C. The freshly prepared diazonium salt solution was then added to this cooled coupling solution. The reaction mixture was maintained in the ice bath for 1.5 hours with continuous stirring. Subsequently, a 10% sodium hydroxide solution (15 mL) was added gradually, and the mixture was poured into ice-cold water (100 mL). The precipitated crude product was collected by filtration, washed thoroughly with water, and recrystallized from ethanol to afford the pure ligand as a dark red powder (3.96 g, 78%). M.p. > 300 °C ;–UV-visible (ethanol) λmax (nm) 220, 206, 258 (π→π*), 363, 420 (n→π*); – IR (V_{max} cm^{-1}): 3266 (O-H), 3050 (N-H), 1652 (C=O), 1490 (N=N), 1270 (C-O), 1153 (C-N); –^{1}H-NMR (400 MHz, DMSO-d_6) : δ 2.01 (6H, *s* , 2x $NHCOCH_3$), 7.00 (2H, *d*, $^2J_{HH}$ 8.8 Hz, 5-H), 7.55 (2H, *dd*, $^2J_{HH}$ 8.8 Hz, $^3J_{HH}$ 2.4 Hz, 6-H), 8.03 (2H, *d*, $^3J_{HH}$ 2.4 Hz, 2-H), 7.99 (4H, *d*, $^2J_{HH}$ 8.4 Hz, 2'-H/6'-H) and 8.09 (4H, *d*, $^2J_{HH}$ 8.4 Hz, 3'-H/5'-H); –^{13}C-NMR (100 MHz, DMSO-d_6,) : δ 24.4 ($NHCOCH_3$), 112.6 (C-2), 118.8 (C-5), 124.0 (C-3'/5'), 127.0 (C-6), 128.4 (C-2'/6'), 130.0 (C-1'), 132.4 (C-1), 138.5 (C-3), 141.9 (C-4'), 151.6 (C-4), 168.6 (C=O). HRMS (ESI+): *m/z* = 515,2048 (calculed 515.2019 for $C_{28}H_{24}N_6O_4Li$, $[M + Li]^+$); Anal. Calculated for $C_{28}H_{24}N_6O_4$ (508.1959): C, 66.13; H, 4.76; N, 16.53. Found C, 66.13; H, 4.71, N, 16.57.

Synthesis of manganese (II) complex 5. Complex **5** was synthesized by reacting the azo ligand **4** (0.15 g, 0.5 mmol) with $MnCl_2{\cdot}4H_2O$ (0.1 g, 0.5 mmol) in dimethyl sulfoxide (DMSO, 10 mL) at room temperature for 24

 ©AUTHOR(S)

hours (Scheme 2). The resulting precipitate was isolated by filtration and washed thoroughly with water followed by a hot ethanol/water (1:1) mixture, yielding of a red powder (0.44 g, 33%) soluble in DMSO. M.p. > 300 °C; –UV-visible (ethanol) λ_{max} (nm): 221, 254 (π→π*) 343 (π→π*, n→π*) 450 (MLCT); –IR (solid, ATR, V_{max}, cm^{-1}): 3500-3100 (O-H), 3075 (N-H), 2932 (C-H), 1660 (C=O), 1490 (N=N), 1270 (C-O), 949 (Mn-O=S), 572 (Mn-O), 437 (Mn-N); –^{1}H-NMR (400 MHz, $CD_3OD/CDCl_3$) : *δ* 2.13 (9H, *s*, 3x$NHCOCH_3$), 2.64 (48H, *s*, 8 x $(CH_3)_2SO$), 8.16-8.12 (*m*, CH aromatic), 7.49-7.44 (*m*, CH aromatic), 7.88 (*m*, CH aromatic), 7.68 (*m*, CH aromatic), 7.97 (*m*, CH aromatic), 7.79 (*m*, CH aromatic), 6.95 (*m*, CH aromatic); –^{13}C-NMR (100 MHz $CD_3OD/CDCl_3$): *δ* 22.3 ($NHCOCH_3$), 38.5 ($(CH_3)_2SO$), 112-150 (C and CH aromatic), 170.1 (C=O); –HRMS (ESI+): *m/z* =1380.6169 ([M – $C_{24}H_{16}N_4O_2$ + 2H]$^{\bullet+}$), 1314 ([M+Li+2H-L]$^+$), 1269 ([M-H_2L-Li-2H_2O]$^+$), 567 ([$C_{17}H_{37}MnN_4O_6S_4$]$^{3\bullet+}$); Anal. Calculated for [$Mn_2(H_2L)_2$(O-DMSO)$_8$].$(Cl)_2(H_2O)_2$: C, 46.07; H, 5.34; N, 9.48; S, 14.47. Found C, 46.17; H, 5.39; N, 9.33; S, 14.58.

Synthesis of magnesium (II) complex 6. Complex **6** was synthesized by refluxing the azo ligand **4** (0.25 g, 0.5 mmol) with $Mg(NO_3)_2{\cdot}6H_2O$ (0.26 g, 1.0 mmol) in dimethyl sulfoxide (DMSO, 10 mL) for 10 hours (Scheme 2). Upon cooling, the reaction mixture was poured into a cold sodium chloride solution and kept in an ice bath to promote precipitation. The crude product was collected by filtration, washed thoroughly with water, and recrystallized from ethanol to afford the complex as a reddish powder (0.65 g, 54%). M.p. > 300 °C; –UV-visible (ethanol) λ_{max} (nm): 221, 254 (π→π*) 343 (π→π*, n→π*) 454 (MLCT); –IR (solid, ATR, V_{max} cm^{-1}): 3518-3167 (O-H), 3088 (NH),1660 (C=O), 1490 (N=N), ~1380 & ~1300 (N-O of NO_3^-), 1270(C-O), 952 (Mn-O=S), 572 (Mn-O); –^{1}H-NMR (400 MHz, $CD_3OD/CDCl_3$): *δ* 2.12 (s, 9H, 3x $COCH_3$), 2.62 (s, 6H, $(CH_3)_2SO$), 6.92-8.16 (m, Ar-H); –^{13}C-NMR (100 MHz $CD_3OD/CDCl_3$): *δ* 22.8 ($NHCOCH_3$), 39.5 ($(CH_3)_2SO$), 112-150 (C and CH aromatic), 170.3 (C=O); –HRMS (ESI+): 736.1742 ([M + 2H]$^{2+}$), 508 ([$C_{28}H_{24}N_6O_4$]$^+$), 718 ([M-OH]$^+$), 678 ([M-HNO_3-OH]$^+$); Anal. Calculated for [$Mg(H_2L)(NO_3)$(O-DMSO)](NO_3): C, 49.03; H, 4.11; N, 15.25; S, 4.36. Found C, 49.18; H, 4.17; N, 15.37; S, 4.47.

Acknowledgements

The authors gratefully acknowledge the financial support for this work. Emmanuel Sopbué Fondjo thanks the German Academic Exchange Service (DAAD) for a personal grant (No. 91691265). Further support was received from the University of Dschang (internal research grant) and the Cameroonian Ministry of Higher Education (special research allocation).

Supplementary Material

^{1}H-NMR, ^{13}C-NMR, COSY, HSQC, HMBC, IR, UV-vis and HRMS data of ligand and metal complexes are provided in the Supplementary Information.

References

1. Pagga, U.; Brown, D. *Chemosphere* **1986**, *15*, 479–491. https://doi.org/10.1016/0045-6535(86)90542-4

 ©AUTHOR(S)

2. Ahmed, A. I.; Yousif E. I. *Pak. J. Med. Health Sci*. **2022**, *16*, 550-–553. https://doi.org/10.53350/pjmhs22167550
3. Khalid, A.; Arshad, M.; Crowley, D. E. *Appl. Microbiol. Biotechnol.* **2007**, *78,* 361–369. https://doi.org/10.1007/s00253-007-1302-4
4. Swapnil, B. D.; Nandkishor, T.S. *Int. J. Adv. Innov. Res*. **2017**, *4*, 18–24.
5. Muhammed, A.H., Sahap, E.H., Farhan, H. M., Sarhan, W.M. *International Journal of Engineering & Technology.* **2014,** *14*, 1–9.
6. Abdallah, S.M. *Arab. J. Chem*. **2012**, *5*, 251–256. https://doi.org/10.1016/j.arabjc.2010.08.019
7. Mohamed, G. G.; Zayed, M. A.; El-Gamel, N. E. A. *Spectrosc. Lett*. **2000***, 33*, 821–832. https://doi.org/10.1080/00387010009350159
8. Fahad, T. A., Rawaa, H. Y. *World Journal of Pharmaceutical Research.* **2016**, *5*, 35–43.
9. Asmaa, A.; Al-hassani, A. H.; Al-Khafagy, A. A.; Ali, M. *World J. Pharm. Res*. **2014**, *3*, 218–231.
10. Graham, G. G.; Davies, M. J.; Day, R. O.; Mohamudally, A.; Scott, K. F. *Inflammopharmacology*. **2013**, *21*, 201–232. https://doi.org/10.1007/s10787-013-0172-x
11. Derek, R. C., Jon, Z., Robert, P. D.. *Molecules*. **2020**, *25*, 3172–3195. https://doi.org/10.3390/molecules25143172
12. Xishi, T.; Wenhua, Z. *Materials*. **2013**, *6*, 3547–3555. https://doi.org/10.3390/ma6083547
13. Austin, B. A.; Gadhia, A. D. *Rare Diseases Epidemiology: Update and Overview.* **2017**, 233–247. https://doi.org/10.1007/978-3-319-67144-4_14
14. Athira, J.; Sindhu, Y.; Sujamol, S.; Mohanan, K. *J. Serb. Chem. Soc*. **2011**, *76*, 249–261. https://doi.org/10.2298/JSC100414025A
15. Mehmet, T. *Asian J. Chem*. **2014**, *26*, 2161–2165. https://doi.org/10.14233/ajchem.2014.16828
16. Eltaboni, F.; Bader, N.; El-Kailany, R.; Elsharif, N.; Ahmida, A. *J. Chem. Rev*. **2022**, *4*, 313–330.
17. Singh, J., Singh, P. *Bioinorg. Chem. Appl*. **2012**, 1–7. https://doi.org/10.1155/2012/104549
18. Sopbué, E. F.; Kemvou, T. R.; Siéwé, D. A.; Tamokou, J. D. D.; Ekom, S. E.; Djeukoua, S. K. D.; Doungmo, G.; Walters, M. E.; Tsopmo, A.; Peter, F. W. S.; Kuiate, J. R. *IOSR-JAC*. **2020**, 13*,* 08–15. https://doi.org/10.9790/5736-1303010815
19. Ziessel, R.; Grosshenny, V.; Hissler, M.; Stroh, C. *Inorg. Chem*. **2004**, *43*, 4262–4271. https://doi.org/10.1021/ic049822d
20. Calligaris, M. *Coord. Chem. Rev*. **1996**, *153*, 83–154. https://doi.org/10.1016/0010-8545(95)01193-5
21. Sirlane, A. A.; Santana, V. P.; Carvalho, Jr.; Benedito, S. L-N. *J. Braz. Chem. Soc*. **2010**, *21*, 279–287
22. Ziessel, R.; Grosshenny, V.; Hissler, M.; Stroh, C. *Inorg. Chem*. **2004**, *43*, 4262–4271. https://doi.org/10.1021/ic049822d
23. Calligaris, M. *Coord. Chem. Rev*. **1996**, *153*, 83–154. https://doi.org/10.1016/0010-8545(95)01193-5
24. Mario, L.; Kyan, A.; Mohammad, M. *Org. Lett.* **2020**. *22*, 8802-8807. https://dx.doi.org/10.1021/acs.orglett.0c03160

 ©AUTHOR(S)

25. Sopbué, F. E.; Siéwé, A. D.; Tamokou, J. D. D.; Ekom, E. S.; Djeukoua, D. S. K.; Doungmo, G.; Walters, E. M.; Tsopmo, A.; Peter, S. W. F.; Kuiate, J. R. *Acta Chemical Slovenica*. **2020**, *67,* 203–211. https://doi.org/10.17344/acsi.2019.5365
26. Sopbué, F. E.; Dennue, K. R.; Tamokou, J. D. D.; Doungmo, G.; Tsopmo, A.; Peter, S. W. F.; Kuiate, J. R. *Am. J. Chem*. **2023**, *13,* 83–95. https://doi.org/10.5923/j.chemistry.20231303.03
27. Akoun, A.; Abdoulaye, D.; Amadou, I. T.; Olivier, O.; Adama, S. *Am. J. Org. Chem.* **2020**, *10*, 1–16. https://doi.org/10.5923/j.ajoc.20201001.01
28. Sheida, E. and Elham, Z. *Acta Chim. Slov.* **2018**, *65*, 416–428. https://doi.org/10.17344/acsi.2018.4159
29. Gatsing, D. and Adoga, G. I. *Res. J. Microbiol*. **2007**, 2, 876–880.
30. Tamokou, J.-de-D.; Kuiate, J.R.; Tene, M.; Tane, P. *Indian J. Pharmacol*. **2009a,** 41, 60–63.
31. Mbah, J.A.; Ayimele, G. A.; Kodjio, N.; Yong, J. N.; Nfor, E. N.; Gatsing, D. *Inter. J. Org. Chem.* **2017**, 7, 229–239. https://doi.org/10.4236/ijoc.2017.73017
32. Mahalakshmi, N., and Rajavel, R. *Arab. J. Chem.* **2014**, *7*, 509–517. https://doi.org/10.1016/j.arabjc.201
33. Tamokou, J. D. D.; Tala, M. F.; Wabo, H. K.; Kuiate, J. R.; Tane, P. *J. Ethnopharmacol.* **2009**, *124*, 571–575. https://doi.org/10.1016/j.jep.2009.04.062
34. Tamokou, J. D. D.; Mbaveng, A.T.; Kuete, V. *Medicinal Spices and Vegetables from Africa*. **2017**, 207–237. https://doi.org/10.1016/b978-0-12-809286-6.00008-x
35. Gehad, G. M.; Walaa, H. M.; Ahmed, M. R. *J. Chem*. **2020**, *2020,* 1–19.

This paper is an open access article distributed under the terms of the Creative Commons Attribution (CC BY) license (http://creativecommons.org/licenses/by/4.0/)